Co-Design of the PV Array and DC/AC Inverter for Maximizing the Energy Production in Grid-Connected Applications

Koutroulis, Eftichios; Yang, Yongheng; Blaabjerg, Frede

Co-Design of the PV Array and DC/AC Inverter for Maximizing the Energy Production in Grid-Connected Applications

Eftichios Koutroulis, *Senior Member, IEEE*, Yongheng Yang, *Senior Member, IEEE*, and

Frede Blaabjerg, *Fellow, IEEE*

Abstract - **Grid-connected Photovoltaic (PV) systems are currently developed by merging a PV array and a DC/AC inverter which are designed separately, without considering the impact of the PV array operational characteristics on the power losses of the DC/AC inverter. In this paper, a co-design technique is presented, where the optimal design parameters of the PV array and DC/AC inverter in a grid-connected PV system are calculated concurrently through a unified design process. The proposed technique enables optimally matching the PV array configuration and the DC/AC inverter structure. A study has been performed, where the PV systems synthesized by applying the proposed co-design technique are compared with PV system configurations comprising PV arrays and DC/AC inverters that have been designed separately, through distinct optimization processes based on various alternative optimization objectives. The design for two installation sites, with different meteorological conditions during a year, demonstrates that only the proposed co-design optimization technique is capable to ensure the maximization of the annual energy production of the overall grid-connected PV system.**

Index Terms- **Photovoltaic (PV) power systems, DC-AC power conversion, Optimization methods, Particle Swarm Optimization (PSO), Renewable Energy Sources (RES).**

I. INTRODUCTION

T HE installation of grid-connected Photovoltaic (PV) systems has followed an exponential growth during the last decades. However, the global installed capacity of PV systems is expected to be further increased in the following years [1]. To pave the way, additional advancements in PV materials, power converters, and control strategies should be achieved. Simultaneously, design for high reliability and high efficiency is an important topic [2].

A general diagram of a grid-connected PV system is depicted in Fig. 1. A PV array is formed by connecting multiple PV cells/modules in series and parallel. The PV array is then connected to a DC/AC inverter that interfaces the PV-generated energy to the electric grid. Transformerless DC/AC inverter topologies (e.g., Neutral Point Clamped - NPC and H6) are lately used in PV applications due to their small volume, light weight, low leakage currents, and high efficiency [3]-[5]. An output filter, consisting of passive

E. Koutroulis is with the School of Electrical and Computer Engineering, Technical University of Crete, Chania GR-73100, Greece (e-mail: efkout@electronics.tuc.gr).

Y. Yang and F. Blaabjerg are with the Department of Energy Technology, Aalborg University, Aalborg DK-9220, Denmark (e-mail: yoy@et.aau.dk; fbl@et.aau.dk).
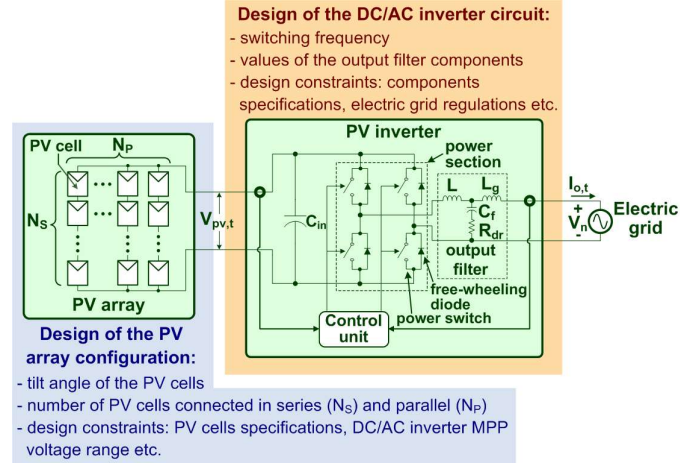
Fig. 1. A block diagram of a grid-connected PV system, where the major design concerns also are listed.

components (i.e., inductors, capacitors, and damping resistors), is used to reduce the harmonic distortion of the injected current. A microelectronic control unit is also employed in the PV inverter structure for implementing processes, such as the Maximum Power Point Tracking (MPPT) of the PV power source and the synchronization with the electric grid [6].

The target of a grid-connected PV system is to inject the maximum possible amount of energy into the electric grid to optimize the corresponding economic benefit achieved during its operation. As illustrated in Fig. 1, in order to develop a grid-connected PV system, two sets of parameters must be considered during the design phase:

(i) the PV array design parameters, such as its tilt angle and the arrangement of PV cells in series/parallel connections;

(ii) the PV inverter design parameters, such as the switching frequency and the passive components of the output filter.

Design techniques have been presented in the literature for calculating the optimal number of PV modules and energy storage units which should be incorporated in stand-alone, or grid-connected PV, or hybrid PV/wind systems, such that the total cost of the overall energy production system is minimized and its reliability is maximized (e.g., in [7], [8]). Additionally, various optimization methodologies for PV systems have been presented in [9]-[11] for the calculation of design parameters such as the optimal tilt angle, the number of PV modules and the number of PV strings. Also, these

techniques enable the optimal selection of PV modules and DC/AC inverters among lists of commercially-available devices. Examples of design optimization objectives are the maximization of the annual solar irradiation on the PV arrays, the maximization of the total energy production during the PV system lifetime period, the maximization of the total economic benefit, and the minimization of the PV plant cost.

Optimization techniques for the design of PV power converters have been presented in [12]-[18]. In [12], the switching frequency and the maximum peak-to-peak current ripple under rated conditions are used as the main design variables. The design target is to optimize the configurations of DC/AC converters connected to the grid in terms of the weighted European efficiency, power density, and cost. The volume or mass of a three-phase two-level DC/AC inverter is optimized in [13] with respect to the switching frequency, the switching device types, the heat sink, as well as the DC-link and output filters. In [14], the switching frequency of three-phase pulse-width modulation (PWM) voltage-source converters is initially selected such that the desired efficiency at the rated power is obtained. The resultant switching frequency is then used to design an LCL-type output filter, in order to achieve the desired quality of the injected current. In [18], the optimal switching frequency and the optimal passive components for the output filter of transformerless grid-connected PV inverters are calculated such that the Levelized Cost Of generated Energy (LCOE) is minimized.

However, all the above design techniques for PV systems have been focused on either exclusively the PV array design considering a predefined PV inverter configuration, or only on the PV inverter design based on generic performance metrics (e.g., the European efficiency), or predefined configurations of PV arrays. Clearly, two separately optimally-designed parts of the PV system (i.e., the PV array and the DC/AC inverter) are merged in the final design. In this case, the energy production performance of the overall PV system is actually not optimal, since the impact of the PV array operational characteristics (e.g., output voltage range) on the inverter power losses. In light of this, a co-design technique is presented in this paper, where the optimal design parameters of the PV array and DC/AC inverter are calculated concurrently through a unified design process. Meteorological conditions of target installation sites during a year are also considered in the proposed design. The scientific contributions of this paper are the following:

1. A design method for PV systems is presented for the first time, where the interdependency of the PV array and DC/AC inverter design parameters and their simultaneous impact on the energy production are considered during the design. Thus, as will be demonstrated in the following, the proposed method enables the optimal matching of the PV array configuration and the DC/AC inverter structure. Consequently, the proposed co-design technique is the only design method available till present which guarantees the maximization of the overall energy production.

2. As described in the above, various optimization objectives have been proposed in the past to design either the PV array or the DC/AC inverter in a PV system. Till present, the impact of the selected objective function on the energy production performance of the overall PV system has not been investigated. To fill this gap, a comparative study is performed in this paper to explore the energy production performance of PV systems, where the PV array and the DC/AC inverter have been separately designed with distinct optimization processes using various optimization objectives. With the proposed co-design method, the upper (maximum) limit of the energy production capability of any PV system is considered. Thus, the comparative results presented are important to assess the effectiveness and optimality of the prior-art design optimization objectives. Therefore, this study provides practical guidelines to achieve the optimal design of PV systems in terms of their energy production performance.

The rest of the paper is organized as follows: the proposed co-design optimization technique is described in § II. The alternative optimization objectives of the comparative study, where the PV array and the DC/AC inverter are designed through distinct optimization processes, are described in § III. Comparative design optimization results for two installation sites in Europe and various objective functions are presented in § IV and, finally, conclusions are drawn in § V.

II. PROPOSED CO-DESIGN OPTIMIZATION METHODOLOGY

A block diagram of the PV system under study is illustrated in Fig. 1. The PV array consists of N_P parallel strings and each string comprises N_S PV cells connected in series. The PV inverter comprises a power section of full-bridge topology with Insulated-Gate Bipolar Transistor (IGBT) power switches and freewheeling diodes, as well as an LCL-type output filter. However, the proposed methodology can be easily modified for other PV inverter topologies, according to the procedure to be described next. The power switches are controlled using the Sinusoidal Pulse Width Modulation (SPWM) technique.

A flowchart of the proposed co-design technique is illustrated in Fig. 2. The input parameters provided by the designer include:

- The PV system specifications: the nominal power rating, latitude and longitude of the installation site, nominal frequency, and Root-Mean-Square (RMS) voltage of the electric grid;
- The operational characteristics (under Standard Test Conditions, STC) of the PV cells, which will be used to synthesize the PV array;
- The operational parameters of the PV inverter components (i.e., power switches and diodes of the power section and output-filter inductors and capacitor), which will be used in the calculation of the PV inverter power losses during the year; and
- The time-series of the hourly-mean solar irradiance levels on the horizontal plane and ambient temperatures, which prevail at the installation site during the year.

In addition, a circuit model of the PV inverter, which has been implemented in the PLECS® software program, is used to calculate the efficiency of the PV inverter as a function of its switching frequency, DC input voltage, and DC input power.
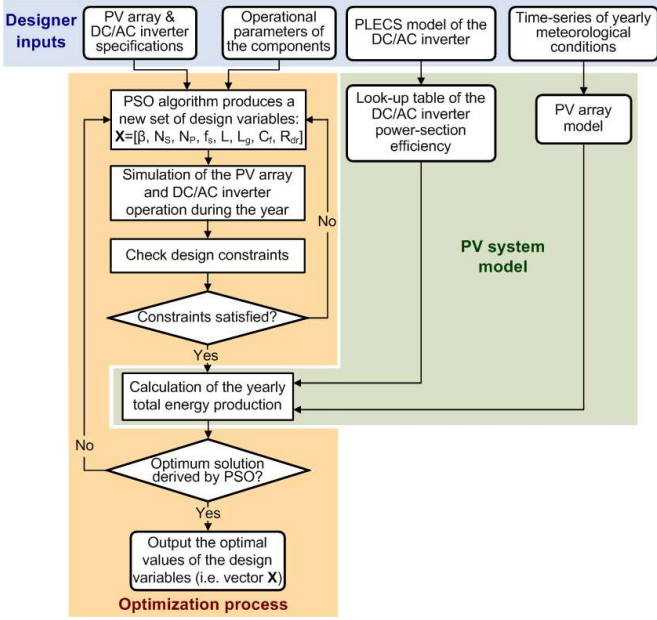
Fig. 2. Flowchart of the proposed optimization process to co-design the PV array and DC/AC inverter (PSO: Particle Swarm Optimization).

The resultant values are stored in a look-up table, which is then used in the optimization process (see Fig. 2), as described next. In order to apply the proposed optimization method to alternative PV inverter topologies (e.g., NPC, H6 etc.), only the model of the power circuit implemented in PLECS® should be modified to calculate the corresponding power conversion efficiencies (then, stored in a look-up table).

The target of the proposed optimization process is to derive the optimal parameters. This includes the PV array tilt angle, β (°), the number of PV cells connected in series, N_S, the number of PV strings connected in parallel, N_P, the switching frequency of the DC/AC inverter power semiconductors, f_s (Hz), as well as the inductances, L and L_g, capacitance, C_f and damping resistance, R_{dr}, of the PV inverter output filter. The optimal design variables are calculated such that the total energy injected into the electric grid during the year, E_y (Wh), is maximized:

$$\underset{X}{maximize}\left\{E_y(X)\right\} \qquad (1)$$

where $X = [\beta, N_S, N_P, f_s, L, L_g, C_f, R_{dr}]$ is the vector of the aforementioned design parameters. It is observed in (1) that the design vector, X, consists of both the PV-array-related and PV-inverter-related design parameters, thus providing the ability to explore their interdependence and their cross-effect on the yearly energy production, E_y, of the overall PV system. The number of parallel PV strings N_P is calculated according to the nominal power rating of the PV system, P_n (W) and the number of series-connected PV cells, as follows:

$$N_P = floor\left(\frac{P_n}{N_S \cdot P_{pvc,STC}}\right) \qquad (2)$$

where $P_{pvc,STC}$ (W) is the power at the Maximum Power Point (MPP) of each PV cell under STC. In the proposed methodology, it is assumed that the control unit of the PV inverter executes an MPPT algorithm, such that the PV cells of the PV array always operate at the corresponding MPP, thus producing the maximum possible power according to the solar irradiation and ambient temperature conditions that prevail at each time instant [19]. The maximum permissible value of N_S, which is calculated during the execution of the proposed optimization process, is constrained such that the MPP voltage generated by the PV array never exceeds the upper limit of the MPP voltage range of the PV inverter, $V_{mpp,max}$ (V), during the yearly operation of the PV system:

$$N_s \leq N_{s,max} = floor\left(\frac{V_{mpp,max}}{V_{pvc,max}}\right) \qquad (3)$$

where:

$$V_{pvc,max} = \underset{1 \leq t \leq 8760}{max}\left\{V_{pvc,t}(\beta, G_t, T_{A,t})\right\} \qquad (4)$$

and $N_{s,max}$ is the maximum permissible number of PV cells connected in series, $V_{pvc,t}$ (V) is the MPP voltage of each PV cell during hour t of the year ($1 \leq t \leq 8760$) and $V_{pvc,max}$ is the maximum among the 8760 different $V_{pvc,t}$ values developed across the PV cells during each hour t of the year. In the proposed methodology, the values of $V_{pvc,t}$ are calculated according to the models presented in [20], by using the value of the tilt angle, β, contained in X, as well as the values of incident solar irradiation on the horizontal plane G_t (W/m^2) and ambient temperature $T_{A,t}$ (°C) during each hour t of the year ($1 \leq t \leq 8760$) which are provided by the designer for the desired installation site.

The annual energy production E_y (Wh) in (1) is calculated by summing the differences between the power produced by the PV array and the total power loss of the PV inverter with a time step of 1 hour during the year:

$$E_y(X) = \sum_{t=1}^{8760}\left(P_{pv,t} - P_{l,t}\right) \cdot \Delta t \qquad (5)$$

where $P_{pv,t}$ (W) is the power produced by the PV array when operating at the MPP during hour t of the year (($1 \leq t \leq 8760$), $P_{l,t}$ (W) is the total power loss of the PV inverter at hour t and $\Delta t = 1$ h is the time step of the energy-production calculations. In case that at any hour t of the year ($1 \leq t \leq 8760$), the MPP voltage produced by the PV array is less than the lower limit of the MPP voltage range of the PV inverter, $V_{mpp,min}$ (V), then the input power of the PV inverter is considered to be zero. Therefore, for each hour t of the year, the value of $P_{pv,t}$ in (5) is calculated as follows:

$$P_{pv,t} = \begin{cases} 0, & \text{if } V_{pv,t} = N_s \cdot V_{pvc,t}(\beta, G_t, T_{A,t}) < V_{mpp,min} \\ N_S \cdot N_P \cdot P_{pvc,t}(\beta, G_t, T_{A,t}), & \text{else} \end{cases} \qquad (6)$$

where $V_{pv,t}$ (V) is the MPP voltage of the PV array and $P_{pvc,t}$ (W) is the MPP power of the PV cells during hour t of the year ($1 \leq t \leq 8760$), which is calculated as a function of β, G_t, and $T_{A,t}$ during the year according to the solar irradiance and PV cells models presented in [20]. Additionally, if the resultant power of $P_{pv,t}$ is higher than the nominal power rating of the PV inverter, P_n (W), then the power provided to the PV inverter, $P_{in,t}$ is curtailed to P_n:

$$P_{in,t} = \begin{cases} P_n & \text{if } P_{pv,t} > P_n \\ P_{pv,t} & \text{else} \end{cases} \qquad (7)$$

The total power loss of the PV inverter during hour t of the year [i.e., $P_{l,t}$ in (5)] consists of the power losses of the PV inverter and output filter (e.g., LCL-type). The total power losses of the PV inverter include the conduction and switching losses of the power devices. The total power loss depends on: (i) the output power and voltage levels produced by the PV array during each hour t of the year ($1 \leq t \leq 8760$) and (ii) the switching frequency of the power devices. Thus, in the proposed methodology, the total power loss of the PV inverter at hour t [i.e., $P_{l,t}$ in (5)] is calculated according to:

$$P_{l,t} = \eta_{ps}(P_{pv,t}, V_{pv,t}, f_s) \cdot P_{pv,t} - P_{LCL,t} - P_c \qquad (8)$$

where $\eta_{ps}(\cdot)$ is the efficiency of the DC/AC inverter power stage, $P_{LCL,t}$ (W) is the total power loss of the output filter during hour t ($1 \leq t \leq 8760$) and P_c (W) is the power consumption of the control unit. The value of P_c is provided by the designer at the beginning of the optimization process. The value of $\eta_{ps}(\cdot)$ is a function of the switching frequency and the PV array MPP output power and voltage levels during each hour t of the year. Its value is calculated by the corresponding values stored in the efficiency look-up table by applying the linear-interpolation technique. The total power losses of the output filter [i.e., $P_{LCL,t}$ in (8)] include the core and winding power losses of the filter inductors (i.e., L and L_g), as well as the power losses of the damping resistor R_{dr} (see Fig. 1). Therefore, the total loss is calculated as

$$P_{LCL,t} = P_{L,c,t} + P_{L,r,t} + P_{Rdr,t} \qquad (9)$$

where $P_{L,c,t}$ (W) is the total core loss of the output filter inductors, $P_{L,r,t}$ (W) is the power loss due to the parasitic resistance of the LCL-filter inductor windings, and $P_{Rdr,t}$ (W) is the power loss of the damping resistor during hour t of the year. The values of $P_{L,c,t}$ and $P_{Rdr,t}$ are calculated as described in [21]. The power loss due to the parasitic resistance of the filter inductor windings, $P_{L,r,t}$ (W), is obtained as

$$P_{L,r,t} = I_{r,t}^2 \cdot r_l \cdot L + I_{o,t}^2 \cdot r_l \cdot (L + L_g) \qquad (10)$$

where r_l (Ω/H) is the parasitic winding resistance per unit inductance, $I_{r,t}$ (A) is the RMS switching ripple due to the converter-side inductance L at hour t and $I_{o,t}$ (A) is the RMS current injected by the PV inverter into the electric grid during hour t of the year ($1 \leq t \leq 8760$).

During the execution of the proposed optimization process, the components of the output filter are selected such that the harmonic distortion of the current injected into the electric grid satisfies the corresponding constraint set by the designer. For this, the ripple factor of the inverter output current, RF (%), is defined as

$$RF = RF_{sw} \cdot R_a \leq RF_{max} \qquad (11)$$

where RF_{sw} (%) is the ripple factor (due to the converter-side inductance, i.e., L in Fig. 1), R_a (%) is the ripple attenuation factor of the LCL filter and RF_{max} (%) is the maximum permissible limit of the output current harmonic distortion. The limit ripple factor RF_{max} in (11) is an input to the proposed optimization process that is provided by the PV system designer. The ripple attenuation factor R_a is calculated

at the switching frequency according to [22]:

$$R_a = \frac{K_d}{\left|1 + \dfrac{L_g}{L} \cdot \left(1 - LC_b \omega_s^2 \dfrac{C_f}{C_b}\right)\right|} \qquad (12)$$

where K_d is a constant factor included in the filter design process considering the reduction of the filter effectiveness due to damping; $C_b = P_n/(2\pi f V_n^2)$ is the base capacitance with V_n (V) being the nominal RMS voltage of the electric grid; and $\omega_s = 2\pi f_{s,r}$ with $f_{s,r}$ (Hz) being the switching frequency of the output voltage of the DC/AC inverter (i.e., input voltage of the LCL-type output filter). $f_{s,r}$ depends on the modulation scheme that is employed by the designer to control the power switches (e.g., $f_{s,r} = f_s$ in a bipolar SPWM and $f_{s,r} = 2 \times f_s$ in a unipolar SPWM) [23]. Then, RF_{sw} in (11) is given by [22]

$$RF_{sw} = \frac{I_{r,t} \cdot V_n}{P_n} \leq RF_{sw,m} \qquad (13)$$

where $RF_{sw,m}$ (%) is the maximum permissible limit of RF_{sw} (typically set between 0.1 and 0.25).

The RMS switching ripple $I_{r,t}$ in (10) and (13) depends on the switching frequency of the PV inverter and the MPP output voltage of the PV array during hour t. In the proposed optimization process, it is calculated following the analysis in [21] and [24]. Furthermore, to avoid resonance, the LCL-filter components are selected such that the resonant frequency of the filter, f_{res} (Hz), is constrained as [22]:

$$10 \cdot f \leq f_{res} \leq \frac{f_{s,r}}{2} \qquad (14)$$

where $f_{res} = \frac{1}{2\pi} \cdot \sqrt{(L + L_g)/L_g C_f L}$ and f (Hz) is the nominal fundamental grid frequency (i.e., $f = 50$ or 60 Hz). In addition, according to the LCL-filter design guidelines presented in [22], the following constraints are imposed on the selection of the output filter components:

$$L + L_g \leq 0.1 \cdot L_b \qquad (15)$$

$$C_f \leq 0.05 \cdot C_b \qquad (16)$$

in which $L_b = V_n^2/(2\pi f P_n)$ is the base inductance. The LCL-filter damping resistor R_{dr} is set to be equal to the impedance of the filter capacitor at the resonant frequency [22]:

$$R_{dr} = \frac{1}{C_f 2\pi f_{res}} \qquad (17)$$

During the execution of the proposed optimization procedure, the switching frequency of the PV inverter is constrained by the maximum, $f_{s,max}$ (Hz), specified by the manufacturers of the power devices:

$$f_s \leq f_{s,max} \qquad (18)$$

As illustrated in Fig. 2, during the execution of the proposed co-design optimization process, alternative designs (i.e., $X = [\beta, N_S, N_P, f_s, L, L_g, C_f, R_{dr}]$) are produced by using the Particle Swarm Optimization (PSO) algorithm. During its execution, the PSO algorithm produces iteratively different sets of the design vector X, which constitute the particles of the swarm under evolution, as described in [25]. For each

generated design vector X by the PSO algorithm, the PV system is simulated for a time period of one year in order to: 1) verify that the optimization constraints defined by (3), (6), (7), (11), (13)-(16) and (18) are satisfied and 2) calculate the yearly energy injected into the electric grid by the PV system [i.e., E_y in (1) and (5)]. If any of the constraints is not satisfied, the corresponding vector, X, is not considered as a potentially optimal solution of the design optimization. This procedure is repeated until it reaches the optimal (i.e., the maximum) annual energy yield E_y in (1).

III. ALTERNATIVE DESIGN OPTIMIZATION OBJECTIVES

For comparison, the performance of alternative PV system configurations has also been investigated, which have been formed by merging a PV array and a PV inverter that have been designed separately through distinct optimization processes. In the design of the PV array and DC/AC inverter in these PV systems, the following optimization objectives have been employed alternatively instead of (1):

- *Optimization objective 1*: the optimal tilt angle of the PV array, β (°), is calculated such that the total solar irradiance on the PV array during the year is maximized:

$$\underset{\beta}{maximize}\left\{\sum_{t=1}^{8760} G_{\beta,t}\right\} \tag{19}$$

where $G_{\beta,t}$ (W/m²) is the solar irradiance during hour t of the year ($1 \leq t \leq 8760$) on the surface of the PV cells installed with a tilt angle of β. Here, $G_{\beta,t}$ in (19) is calculated using the corresponding solar irradiance level on the horizontal plane G_t (W/m²) input by the designer to the optimization algorithm, according to the models in [20]. When executing the optimization in (19), the MPPT voltage range of the PV inverter is not considered to calculate the optimal tilt angle β.

- *Optimization objective 2*: the optimal switching frequency, f_s, and optimal output filter components (i.e., L, L_g, C_f, and R_{dr}) are calculated such that the average European efficiency [3] of the PV inverter is maximized. The average European efficiency is calculated considering the inverter operation at three DC input voltage levels, which are located around the midpoint of the MPP voltage range:

$$\underset{X_1}{maximize}\left\{\sum_{i=1}^{3} \eta_{EU,i}(X_1,V_{pv,i}) \middle/ 3\right\} \tag{20}$$

where $X_1 = [f_s, L, L_g, C_f, R_{dr}]$ is the vector of design variables and $\eta_{EU,i}$ is the European efficiency of the PV inverter when operating with a DC input voltage equal to $V_{pv,i}$ (V). The three voltage levels in (20) have been set equal to $V_{pv,i} = V_{mpp,min} + k_i \cdot \Delta V_{mpp}$, where $k_1 = 0.31$, $k_2 = 0.43$, and $k_3 = 0.56$, similarly to [12] and $\Delta V_{mpp} = V_{mpp,max} - V_{mpp,min}$. The optimal vector X_1 is calculated to ensure that the objective function of (20) is maximized and simultaneously the constraints (11), (13)-(16) and (18) are satisfied.

- *Optimization objective 3*: the optimal design variables $X_1 = [f_s, L, L_g, C_f, R_{dr}]$ is calculated such that the average European efficiency of the PV inverter is maximized, when operating at three DC input voltage levels that cover the entire MPP voltage range:

$$\underset{X_1}{maximize}\left\{\sum_{i=1}^{3} \eta_{EU,i}(X_1,V_{pv,i}) \middle/ 3\right\} \tag{21}$$

where $V_{pv,i}$ has been set equal to $V_{mpp,min}$, $V_{mpp,min} + \Delta V_{mpp}/2$, and $V_{mpp,max}$, respectively. The optimal vector X_1 is calculated in a way that the objective function of (21) is maximized and also the design constraints (11), (13)-(16) and (18) are met. The average European efficiency of the PV inverter in (21) is calculated at three specific operating MPP voltage levels of the PV array, which, however, are located over a broader range compared to those in the optimization objective 2.

- *Optimization objective 4*: the optimal design vector $X_1 = [f_s, L, L_g, C_f, R_{dr}]$ is calculated such that the maximum value of European efficiency that is exhibited by the PV inverter when operating over the entire MPP input voltage range (i.e., from $V_{mpp,min}$ to $V_{mpp,max}$) is maximized:

$$\underset{X_1}{maximize}\left\{\max\left[\eta_{EU,i}(X_1,V_{pv,i})\right]_{V_{pv,i}=V_{mpp,min}}^{V_{pv,i}=V_{mpp,max}}\right\} \tag{22}$$

In order to perform the optimization process described by (22), the values of $\eta_{EU,i}(X_1, V_{pv,i})$ are calculated for all values of the MPP input voltage range of the PV inverter, $V_{pv,i}$, in the range from $V_{mpp,min}$ to $V_{mpp,max}$ with a voltage step of 10 V. In addition, during the execution of this optimization process, it is checked that the constraints (11), (13)-(16) and (18) are also satisfied. Compared to optimization objectives 2 and 3, in this objective, the optimization algorithm targets to derive the maximum European efficiency that is exhibited at any MPP voltage level within the range from $V_{mpp,min}$ to $V_{mpp,max}$.

- *Optimization objective 5*: the optimal values of the filter components are calculated such that the power conversion efficiency of the PV inverter (including the power stage and output filter) is maximized when operating at the nominal DC input power and voltage levels:

$$\underset{X_2}{maximize}\left\{\eta(X_2,V_{mpp,max},P_n)\right\} \tag{23}$$

where $X_2 = [L, L_g, C_f, R_{dr}]$ is the vector of design parameters in this objective function and $\eta(\cdot)$ is the power conversion efficiency of the PV inverter. Here, $\eta(\cdot)$ is evaluated at the DC input voltage and power levels $V_{mpp,max}$ and P_n, respectively. In this optimization objective, the switching frequency of the PV inverter has been set as 10 kHz [4], while the optimization process is executed such that the design constraints (11) and (13)-(16) are satisfied.

- *Optimization objective 6*: the optimal tilt angle β of the PV array and the optimal number of PV cells in series and parallel (i.e., N_S and N_P, respectively) are calculated such that the total energy injected by the PV system into the electric grid is maximized:

$$\underset{X_3}{maximize}\left\{E_y(X_3)\right\} \tag{24}$$

where $X_3 = [\beta, N_S, N_P]$ is the vector of the optimization design variables. The constraints in this case are given by (3), (6) and (7). This optimization objective is applied for PV systems comprising a PV inverter that has already been optimized separately according to the aforementioned alternative optimization objectives *2-4* [i.e., using objective functions

(20), (21) or (22), respectively].

- Optimization objective 7: the optimal value of $X_3 = [\beta, N_S, N_P]$ is calculated such that the total energy production of the PV array only (i.e., without including the PV inverter) during the year is maximized:

$$\underset{X_3}{maximize}\left\{E_{pv}(X_3)\right\} = \underset{X_3}{maximize}\left\{\sum_{t=1}^{8760} P_{pv,t} \cdot \Delta t\right\} \quad (25)$$

where E_{pv} (Wh) is the total energy produced by the PV array during the year. This optimization process is executed such that the constraints (3), (6) and (7) are also satisfied. When implementing this optimization objective, it is considered that the PV system contains a PV inverter that has already been optimized separately according to the alternative optimization objectives *2-4* [i.e., using objective functions (20), (21) or (22), respectively].

- Optimization objective 8: the optimal value of $X_3 = [\beta, N_S, N_P]$ is calculated such that only the total energy yield of the PV array (i.e., without the PV inverter) during the year is maximized for a PV system. In this case, the PV system comprises a PV inverter that has been optimized separately such that it exhibits the maximum possible efficiency when operating at the nominal DC input MPP power and voltage levels, according to the optimization objective *5* [i.e., using objective function (23)]. The optimal vector X_3 is calculated such that the constraints (3), (6) and (7) are satisfied. The target of both optimization objectives *7* and *8* is only to derive the optimal configuration of the PV array, but they differ due to the optimization objectives which have been previously employed to design the DC/AC inverter of the PV system.

In order to perform the design of PV systems by applying the alternative optimization objectives *1-8*, the optimal β or optimal design parameters X_1 - X_3, are calculated by applying the PSO algorithm, such that the objective functions (19)-(25) are maximized and simultaneously the corresponding design constraints described above are satisfied.

Comparative optimization results of the PV system configuration and energy production, which are derived by alternatively optimizing the objective functions (1) and (19)-(25), respectively, are presented in the following section.

IV. DESIGN OPTIMIZATION RESULTS

The proposed methodology has been applied to optimally co-design the PV array and DC/AC inverter of the PV system shown in Fig. 1 with the nominal power rating being $P_n = 1.6$ kW. The PV system is interconnected to an electric grid with $V_n = 220$ V (RMS) and $f = 50$ Hz. The operational characteristics of the PV cells that were used by the optimization algorithm to synthesize the PV array of the PV system are shown in Table I. The MPP voltage range of the PV inverter is from $V_{mpp,min} = 350$ V to $V_{mpp,max} = 600$ V. The PV inverter consists of IGBT-type power switches and power diodes with $f_{s,max} = 15$ kHz. The power consumption of the control unit in (4) has been set as $P_c = 5$ W. The proposed optimization process has been implemented in the MATLAB® software platform according to the description in § II. A model of the PV inverter in the PLECS® software

TABLE I
OPERATIONAL CHARACTERISTICS OF THE PV CELLS UNDER STC.

MPP power	0.556 W
Open-circuit voltage	0.583 V
Short-circuit current	1.29 A
Temperature coefficient of open-circuit voltage	0.0021 ºC/V
Temperature coefficient of short-circuit current	0.0013545 A/ºC
Nominal operating cell temperature (NOCT)	47 ºC

program has been used to calculate the efficiency of the power section of the PV inverter as a function of its DC input power, DC input voltage, and switching frequency with steps of 40 W, 25 V and 2.5 kHz, respectively. The resultant values are then used to build up a look-up table for the execution of the proposed co-design optimization process, as described in § II. The proposed co-design optimization process has been implemented by using the built-in function of the PSO algorithm that is available in the Global Optimization Toolbox of MATLAB®. The PSO algorithm was set to operate with a swarm size of 250 particles and a maximum number of 3000 iterations. In addition, in order to reduce the execution time of the optimization process, the PSO algorithm operation was set to end when the relative change in the best value of E_y in (1), which was derived during the last 50 iterations, was less than 10^{-6}. The same MATLAB® function and PSO algorithm settings were also used for the maximization of objective functions (19)-(25) to implement the PV system design according to the alternative optimization objectives described in § III. The time required to derive the optimal value of (1) with $X = [\beta, N_S, N_P, f_s, L, L_g, C_f, R_{dr}]$, which is the most computationally complicated among the alternative design objectives in this paper, is approximately one hour for a computer with a 1.7-GHz Central Processing Unit (CPU) and 4-GB of Random Access Memory (RAM). The proposed optimization process is executed: (i) automatically and without any other involvement of the designer except the definition of the optimization algorithm input values, (ii) offline prior to the installation of the actual PV system, and (iii) without any hardware cost overhead. Therefore, this computation time is not significant when compared to the time required to perform the PV system design process manually and also considering the energy production benefit that is achieved. The separately-optimized PV systems are designed by executing two different optimization algorithms (i.e., for the PV array and the DC/AC inverter, respectively). The time required for accomplishing their design is not significantly shorter than that of the proposed co-design technique, but, as will be demonstrated in the following, the design solutions result in less energy production by the PV system.

The results when applying the proposed co-design method for PV systems installed in Chania (Greece) and Oslo (Norway), respectively, are illustrated in Table II. The synthesis of a separately-optimized PV system has also been performed, which, according to the design criteria typically applied in conventional PV installations, comprises a PV array and a DC/AC inverter designed according to the optimization objectives *1* and *5*, respectively, what have been described in § III. In contrast to the proposed co-design technique, where

TABLE II
DESIGN OPTIMIZATION RESULTS FOR 1.6-kW PV SYSTEMS
INSTALLED AT TWO DIFFERENT SITES IN EUROPE.

Optimized PV system through the co-design (proposed) method:

Installation site	Optimal values of the design variables (i.e., $X = [\beta, N_S, N_P, f_s, L, L_g, C_f, R_{dr}]$)							
	β (°)	N_S	N_P	f_s (kHz)	L (mH)	L_g (μH)	C_f (μF)	R_{dr} (Ω)
Chania (Greece)	27.093	960	3	14.95	1.472	47.812	5.261	2.967
Oslo (Norway)	43.284	960	3	14.95	1.559	47.802	5.261	2.969

Separately-optimized PV system based on optimization objectives *1* and *5*:

Chania (Greece)	28.073	960	3	10.00	2.475	106.990	5.261	4.415
Oslo (Norway)	48.610							

TABLE III
ALTERNATIVE PV SYSTEM CONFIGURATIONS SYNTHESIZED BY
COMBINING VARIOUS DESIGN OPTIMIZATION OBJECTIVES OF § III.

PV system configuration no.	Optimization objectives	
	PV array	PV inverter
1	*6*	*2*
2	*6*	*3*
3	*6*	*4*
4	*7*	*2*
5	*7*	*3*
6	*7*	*4*
7	*8*	*5*

TABLE IV
DESIGN RESULTS FOR THE 1.6-kW PV SYSTEM CONFIGURATIONS IN TABLE III
INSTALLED IN OSLO (NORWAY).

PV system configuration no.	Optimal values of the design variables							
	β (°)	N_S	N_P	f_s (kHz)	L (mH)	L_g (μH)	C_f (μF)	R_{dr} (Ω)
1	43.284	960	3	14.95	1.656	47.793	5.261	2.971
2	43.284	960	3	15.00	1.650	47.474	5.261	2.962
3	43.284	960	3	15.00	1.650	47.474	5.261	2.962
4	43.284	960	3	14.95	1.656	47.793	5.261	2.971
5	43.284	960	3	15.00	1.650	47.474	5.261	2.962
6	43.284	960	3	15.00	1.650	47.474	5.261	2.962
7	43.284	960	3	10.00	2.475	106.990	5.261	4.415

TABLE V
DESIGN RESULTS FOR THE 1.6-kW PV SYSTEM CONFIGURATIONS IN
TABLE III INSTALLED IN CHANIA (GREECE).

PV system configuration no.	Optimal values of the design variables							
	β (°)	N_S	N_P	f_s (kHz)	L (mH)	L_g (μH)	C_f (μF)	R_{dr} (Ω)
1	27.093	960	3	14.95	1.656	47.793	5.261	2.971
2	27.084	960	3	15.00	1.650	47.474	5.261	2.962
3	27.084	960	3	15.00	1.650	47.474	5.261	2.962
4	27.108	960	3	14.95	1.656	47.793	5.261	2.971
5	27.108	960	3	15.00	1.650	47.474	5.261	2.962
6	27.108	960	3	15.00	1.650	47.474	5.261	2.962
7	27.108	960	3	10.00	2.475	106.990	5.261	4.415

the optimal values of all design parameters are calculated concurrently by the optimization algorithm, the values of N_S and N_P in the separately-optimized PV system must be selected by the designer, since they are not considered when evaluating the objective functions (19) and (23), respectively. For the separately-optimized PV system presented in Table II, N_S = 720 and N_P = 4 were selected, thus satisfying (2). The simulation results indicate that the energy production of the PV system would drop by 68.3 % and 91.4 % for the installation sites of Oslo and Chania, respectively, compared to the case with N_S = 960 and N_P = 3. This is due to the high number of operating hours outside the MPP voltage range of the PV inverter, which results in zero energy production according to (6). Therefore, in the design results presented in Table II, N_S= 960 and N_P = 3 have been adopted to synthesize the separately-optimized PV system. These values, which are also equal to those of the optimally co-designed counterpart in Table II, enable to identify the upper (i.e. maximum) limit of energy production capability of the separately-optimized PV system and investigate the impact of the optimization objectives *1* and *5* on the energy production. It is observed in Table II that different sets of optimal design parameters have been derived in each installation site, due to the different meteorological conditions prevailing during the year. Since the values of inductors and filter damping resistor are lower in the optimized designs, the total cost of the optimized PV systems is lower than the cost of the separately-optimized counterpart based on optimization objectives *1* and *5*.

The performances of alternative PV system configurations, which are synthesized by separately-designed PV arrays and PV inverters based on combinations of the optimization objectives described in § III, have also been investigated. The resultant PV system configurations are presented in Table III. The corresponding design results for PV systems installed in Chania (Greece) and Oslo (Norway) are presented in Tables IV and V, respectively. In all PV system configurations investigated in Tables II-V, the optimal number of PV cells connected in series in each PV string of the PV array, N_S, is less than the corresponding maximum permissible values of $N_{S,max}$=1035 for Oslo and $N_{S,max}$=1104 for Chania, thus satisfying (3). The resultant optimal N_S ensures that the number of hours of PV inverter operation with a DC input voltage lower than $V_{mpp,min}$ according to (6) and the associated loss of PV energy production, are minimized (e.g., compared to the case that N_S =720 was selected). The application of the PV array design optimization objectives *6-8* described in § III, resulted in the same value of N_S for both installation sites, since the MPPT voltage range [defined by $V_{mpp,min}$ and $V_{mpp,max}$, respectively, in (3) and (6)] is also considered when calculating the corresponding objective functions [i.e., (24) and (25) in § III]. After that selection of N_S, the number of PV strings connected in parallel, N_P, was calculated such that the desired nominal power rating of the entire PV system (i.e. P_n = 1.6 kW), which has been specified by the designer as an input of the design process, is obtained.

The tilt angle of the PV array affects the solar irradiance actually received by the PV cells, which, in turn, affects the MPP voltage and the generated power. The optimization objectives *7* and *8* in § III, do not consider the impact of the MPP voltage and power levels produced by the PV array on the inverter energy production efficiency. In contrast, the

optimization objective *6* indirectly considers this aspect through the maximization of the energy production of the entire PV system. Thus, slightly different values of the PV cells tilt angle, *β*, have been derived when employing the PV array design optimization objective *6* compared to the design objectives *7* and *8* for the installation site of Chania, where both the solar irradiation and ambient temperature are higher compared to the installation site of Oslo. The optimal values of *β* are the same for all alternative PV system configurations for the installation site of Oslo, mainly because of the low solar irradiation potential of that location. Furthermore, identical optimal values of the LCL-type filter capacitance, C_f, have been derived for all PV configurations presented in Tables II-V, which, additionally, are approximately equal to the corresponding maximum permissible limit imposed by (16). This approach, in combination with the selection of a high switching frequency, enabled the optimization algorithm to reduce the inductances *L* and L_g of the output filter, resulting in a reduction of the associated power losses of the PV inverter and an increase of the electric energy injected into the electric grid. In both installation sites, a different PV inverter structure has been derived when the optimization objective *2* was applied, compared to the objectives *3* and *4*, since, in that case, the average European efficiency over a narrower DC input voltage range of the PV inverter was maximized. Furthermore, in both installation sites, the application of optimization objectives *3* and *4* for the design of the DC/AC inverter, resulted in the same values of the design variables, irrespectively of the optimization objective employed to design the PV array (i.e., objectives *6* or *7*, respectively, in Tables IV and V). This result is due to the low sensitivity of the PV inverter European efficiency with the MPP output voltage of the PV array.

The total energy injected into the electric grid for the installation sites of Oslo and Chania, by the PV systems presented in Tables II-V, is illustrated in Fig. 3. The PV system configuration number provided in Table III is used as a reference in Fig. 3. The energy production performance of the PV system configuration no. *7* is significantly lower than both the energy production of the PV system derived by applying the proposed co-design technique and the PV system configurations no. *1-6*, for both installation sites. Thus, it is concluded that the optimization of the PV inverter considering only the nominal DC input voltage and power levels is not adequate to ensure the maximization of the overall PV system energy production, since the MPP voltage and power of a PV array change continuously during the year. Furthermore, when comparing the energy production of the separately-optimized configuration presented in Table II with the PV system configuration no. *7*, an interesting conclusion can be drawn. That is, selecting the PV array design parameters considering only the incident solar irradiation during the year (without taking into account the MPP voltage range of the PV inverter) results in a deterioration of the annual energy production capability of the overall PV system.

The results presented in Fig. 3 demonstrate that the total energy production of the PV systems designed by employing
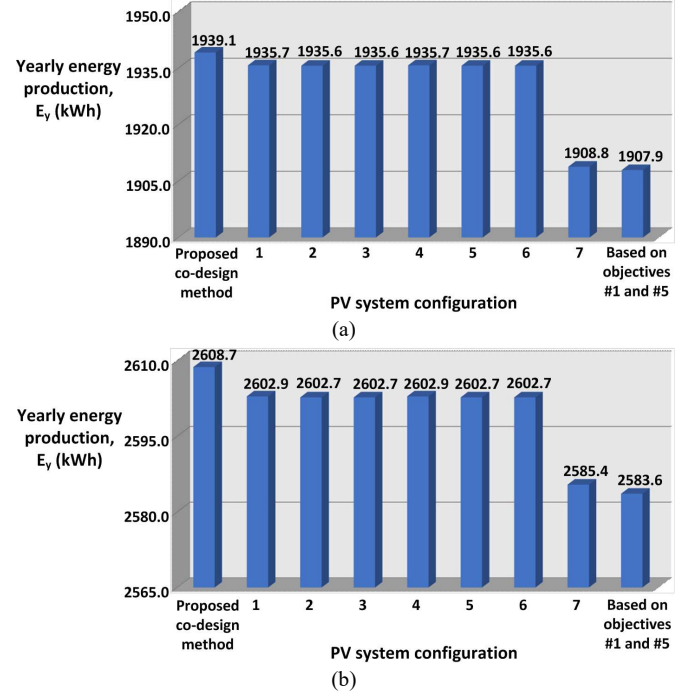

Fig. 3. The total energy injected into the electric grid by the PV systems designed when applying the proposed co-design optimization methodology and the alternative design optimization objectives presented in Tables II-III, respectively: (a) for the installation site of Oslo (Norway) and (b) for the installation site of Chania (Greece).

the proposed co-design methodology is higher by 0.18-1.64 % for the installation site of Oslo and by 0.22-0.97 % for the installation site of Chania. Therefore, by applying the proposed co-design optimization technique enables to derive PV system configurations which are capable to inject more energy into the electric grid compared to the PV systems formed by merging separately designed PV arrays and PV inverters, even if these two subsystems had been previously designed through individual optimization processes. The minimum deviation from the energy production enabled by the PV systems designed through the proposed co-design technique is achieved in both installation sites by configurations no. 1 and no. 4. Although a different design objective has been applied in order to design the PV arrays of these two configurations (see Table III), both of them have been derived by employing objective *2* for the optimal design of the PV inverter. This optimization objective is based on the maximization of the European efficiency over a narrower DC input voltage range compared to that considered in the PV inverter design objectives *3* and *4*, which better matches the actual MPP voltage levels produced by the PV array during the year at the installation sites under consideration. In addition, although the energy produced by configurations no. *1-6* is higher than that of the configurations comprising a DC/AC inverter optimized for the maximum efficiency at the nominal DC input voltage and power, only the proposed co-design technique ensures the maximization of the annual energy production of the total PV system.

Overall, the results presented in Tables II-V and Fig. 3 demonstrate that:

1. The optimal design parameters depend on the type of

objective function, which is applied to design the PV system. When employing the alternative optimization objectives for the separate designs, the maximum absolute deviations of the resultant designs (β, f_s, L, L_g and R_{dr}) from the corresponding values derived by the proposed co-design method (Tables II and IV-V) are 12.30%, 33.11%, 58.76%, 123.82%, and 48.70%, for Oslo. Those deviations are 3.62%, 33.11%, 68.14%, 123.77% and 48.80%, for Chania.

2. The optimal PV system design parameters depend on the meteorological conditions of the installation site. For each optimization objective investigated in Tables II-V, the resultant designs (β, L and R_{dr}) that have been derived for Oslo exhibit a maximum deviation from the corresponding designs for Chania by 73.15%, 5.91% and 0.07%.

3. Even for the same configuration of the PV array in terms of β, N_S and N_P (e.g., for Oslo in Tables II and IV), the PV inverter structure (i.e., in terms of [f_s, L, L_g, C_f, R_{dr}]) matches differently to the yearly outputs of the PV source (determined by [β, N_S, N_P]), depending on the employed optimization objective. Furthermore, the results shown in Fig. 3 reveal that only the proposed co-design technique achieves the optimal PV-array/PV-inverter matching, contributing to the maximization of the PV energy yield.
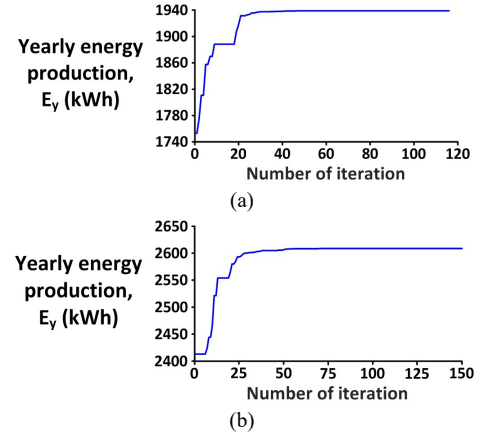
An example of the evolution of the proposed PSO-based co-design process is presented in Fig. 4. It is depicted in Fig. 4 that the best values of the objective function E_y in (1) were derived after the evaluation of all swarm particles at the end of each iteration. It is also observed that a near-optimum solution is derived during the early stages of the PSO algorithm execution, due to: (i) the large number of particles comprising the swarm of potential solutions, which enables to explore a large part of the search-space in each iteration and (ii) the effectiveness of the PSO algorithm to solve complex optimization problems by effectively producing the alternative potential solutions of the optimization problem, which are explored during each iteration.

V. CONCLUSIONS

The continuous growth of the global PV market expected in the following years necessitates the further improvement of the PV systems efficiency in order to promote their competitiveness over alternative energy technologies. Currently, to develop grid-connected PV systems, two separately designed parts—the PV array and the DC/AC inverter—are merged. This approach has the disadvantage that the impact of the PV array operational characteristics (e.g., output voltage range) on the power losses of the DC/AC inverter circuit is not considered when implementing the design of these two subsystems.

In this paper, a co-design technique has been presented, where the optimal values of the design parameters of the PV array and DC/AC inverter in a grid-connected PV system are calculated concurrently in a unified design process. Compared to the existing design approaches of PV systems, the proposed optimization technique enables the optimal matching of the PV array configuration and the DC/AC inverter structure.

Fig. 4. The best values of the objective function E_y in (1) during the evolution of the proposed PSO-based co-design process: (a) for the installation site of Oslo (Norway) and (b) for the installation site of Chania (Greece).

Simultaneously, the annual meteorological conditions of the target installation site are considered. A comparative study has been performed, where alternative PV system configurations have also been considered, which comprise PV arrays and DC/AC inverters that have been separately designed through distinct optimization processes based on various alternative optimization objectives. The design results for two installation sites with different meteorological conditions demonstrated the effectiveness of the proposed co-design method. That is, by simultaneously co-designing the PV array and DC/AC inverter enables to derive PV system configurations which are capable to inject more energy into the electric grid compared to the PV systems formed by merging separately designed subsystems (arrays and inverters), even if these subsystems have been previously designed under individual optimization.

VI. REFERENCES

[1] "Global Market Outlook for Solar Power / 2017-21", SolarPower Europe, 2017.
[2] A. Sangwongwanich, Y. Yang, D. Sera, and F. Blaabjerg, "Lifetime evaluation of grid-connected PV inverters considering panel degradation rates and installation sites", *IEEE Trans. Power Electron.*, vol. 33, no. 2, pp. 1225 – 1236, 2018.
[3] H. Jedtberg, A. Pigazo, M. Liserre, and G. Buticchi, "Analysis of the robustness of transformerless PV inverter topologies to the choice of power devices", *IEEE Trans. Power Electron.*, vol. 32, no. 7, pp. 5248-5257, 2017.
[4] T.K.S. Freddy, N.A. Rahim, W.-P. Hew, and H.S. Che, "Comparison and analysis of single-phase transformerless grid-connected PV inverters", *IEEE Trans. Power Electron.*, vol. 29, no. 10, pp. 5358-5369, 2014.
[5] G. E. Valderrama, G. V. Guzman, E. I. Pool-Mazún, P. R. Martinez-Rodriguez, M. J. Lopez-Sanchez, and J. M. Sosa Zuñiga, "A single-phase asymmetrical T-type five-level transformerless PV inverter", *IEEE J. Emerg. Sel. Top. Power Electron.*, vol. 6, no. 1, pp. 140-150, 2018.
[6] N. E. Zakzouk, A. K. Abdelsalam, A. A. Helal, and B. W. Williams, "PV single-phase grid-connected converter: DC-link voltage sensorless prospective," *IEEE J. Emerg. Sel. Top. Power Electron.*, vol. 5, no. 1, pp. 526-546, 2017.
[7] S.K.K. Ng, J. Zhong, and J.W.M. Cheng, "Probabilistic optimal sizing of stand-alone PV systems with modeling of variable solar radiation and load demand", in *Proc. of the Annual IEEE PES General Meeting*, pp. 1-7, 2012.
[8] M. Alsayed, M. Cacciato, G. Scarcella, and G. Scelba, "Multicriteria optimal sizing of Photovoltaic-Wind turbine grid connected systems", *IEEE Trans. Energy Convers.*, vol. 28, no. 2, pp. 370-379, 2013.

[9] A. Aronescu and J. Appelbaum, "Design optimization of photovoltaic solar fields - insight and methodology", *Renewable and Sustainable Energy Reviews*, vol. 76, pp. 882-893, 2017.

[10] T. Kerekes, E. Koutroulis, D. Sera, R. Teodorescu, and M. Katsanevakis, "An optimization method for designing large PV plants", *IEEE J. Photovoltaics*, vol. 3, no. 2, pp. 814-822, 2013.

[11] S.A. Arefifar, F. Paz, and M. Ordonez, "Improving solar power PV plants using multivariate design optimization", *IEEE J. Emerg. Sel. Top. Power Electron.*, vol. 5, no. 2, pp. 638-650, 2017.

[12] R.M. Burkart and J.W. Kolar, "Comparative life cycle cost analysis of Si and SiC PV converter systems based on advanced η-ρ-σ multiobjective optimization techniques", *IEEE Trans. Power Electron.*, vol. 32, no. 6, pp. 4344-4358, 2017.

[13] I. Laird, X. Yuan, J. Scoltock, and A. J. Forsyth, "A design optimization tool for maximizing the power density of 3-phase DC–AC converters using silicon carbide (SiC) devices", *IEEE Trans. Power Electron.*, vol. 33, no. 4, pp. 2913-2932, 2018.

[14] E. Kantar and A. M. Hava, "Optimal design of grid-connected voltage-source converters considering cost and operating factors", *IEEE Trans. Ind. Electron.*, vol. 63, no. 9, pp. 5336-5347, 2016.

[15] A. C. Nanakos, G. C. Christidis, and E. C. Tatakis, "Weighted efficiency optimization of flyback microinverter under improved boundary conduction mode (i-BCM)", *IEEE Trans. Power Electron.*, vol. 30, no. 10, pp. 5548-5564, 2015.

[16] S. Vighetti, J.-P. Ferrieux, and Y. Lembeye, "Optimization and design of a cascaded DC/DC converter devoted to grid-connected photovoltaic systems", *IEEE Trans. Power Electron.*, vol. 27, no. 4, pp. 2018-2027, 2012.

[17] M. Mirjafari, R. S. Balog, and R. Turan, "Multiobjective optimization of the DC–DC stage of a module-integrated inverter based on an efficiency usage model", *IEEE J. Photovoltaics*, vol. 4, no. 3, pp. 906-914, 2014.

[18] S. Saridakis, E. Koutroulis, and F. Blaabjerg, "Optimization of SiC-based H5 and Conergy-NPC Transformerless PV Inverters", *IEEE J. Emerg. Sel. Top. Power Electron.*, vol. 3, no. 2, pp. 555-567, 2015.

[19] S. Maity and M. V. G. Varaprasad, "An efficient PV power optimizer with reduced EMI effects: map-based analysis and design technique", *IEEE Trans. Energy Convers.*, to be published.

[20] E. Lorenzo, "Solar electricity - engineering of photovoltaic systems," 1st ed., PROGENSA, 1994.

[21] E. Koutroulis and F. Blaabjerg, "Methodology for the optimal design of transformerless grid-connected PV inverters", *IET Power Electronics*, vol. 5, no. 8, pp. 1491-1499, 2012.

[22] M. Liserre, F. Blaabjerg, and S. Hansen, "Design and control of an LCL-filter-based three-phase active rectifier", *IEEE Trans. Ind. Appl.*, vol. 41, no. 5, pp. 1281-1291, 2005.

[23] N. Mohan, T. M. Undeland and W. P. Robbins, "Power Electronics: converters, applications, and design", 3rd ed. New York, NY, USA: Wiley, 2002.

[24] H. Kim and K.-H. Kim, "Filter design for grid connected PV inverters", in *Proc. of IEEE Int'l Conf. Sustainable Energy Technologies*, pp. 1070-1075, 2008.

[25] R. B. A. Koad, A. F. Zobaa, A. El-Shahat, "A novel MPPT algorithm based on Particle Swarm Optimization for photovoltaic systems," *IEEE Trans. on Sustainable Energy*, vol. 8, no. 2, pp. 468-476, 2017.

VII. BIOGRAPHIES

Eftichios Koutroulis (M'10–SM'15) was born in Chania, Greece, in 1973. He received the B.Sc. and M.Sc. degrees in electronic and computer engineering, in 1996 and 1999, respectively, and the Ph.D. degree in the area of power electronics and renewable energy sources (RES) from the School of Electronic and Computer Engineering, Technical University of Crete, Chania, in 2002. He is currently an Associate Professor in the School of Electrical and Computer Engineering, Technical University of Crete. His research interests include power electronics, the development of microelectronic energy management systems for RES and the design of photovoltaic and wind energy conversion systems.

Yongheng Yang (S'12–M'15-SM'17) received the B.Eng. degree from Northwestern Polytechnical University, China, in 2009 and the Ph.D. degree from Aalborg University, Denmark, in 2014. He was a postgraduate student with Southeast University, China, from 2009 to 2011. In 2013, he was a Visiting Scholar at Texas A&M University, TX, USA. Since 2014, he has been with the Department of Energy Technology, Aalborg University, where currently he is an Associate Professor. His research includes grid integration of renewable energies, power electronic converter design, analysis and control, and reliability in power electronics. Dr. Yang served as a Guest Associate Editor of IEEE Journal of Emerging and Selected Topics in Power Electronics. He is an Associate Editor of the CPSS Transactions on Power Electronics and Applications and an Editor of the Mathematical Problems in Engineering. Dr. Yang received the 2018 *IET Renewable Power Generation* Premium Award.

Frede Blaabjerg (S'86–M'88–SM'97–F'03) received the Ph.D. degree in electrical engineering from Aalborg University, Aalborg, Denmark, in 1995. He was with ABB-Scandia, Randers, Denmark, from 1987 to 1988. He joined Aalborg University as an Assistant Professor in 1992, an Associate Professor in 1996, and a Full Professor of power electronics and drives in 1998. His current research interests include power electronics and its applications such as wind turbines, PV systems, reliability engineering, power quality, and adjustable speed drives. Prof. Blaabjerg received 18 IEEE Prize Paper Awards, the IEEE PELS Distinguished Service Award in 2009, the EPE-PEMC Council Award in 2010, the IEEE William E. Newell Power Electronics Award 2014 as well as the Villum Kann Rasmussen Research Award 2014. In 2017, he became Villum Investigator. He was the Editor-in-Chief of the IEEE TRANSACTIONS ON POWER ELECTRONICS from 2006 to 2012. In 2014, 2015, and 2016, he was nominated by the Thomson Reuters to be among the most 250 cited researchers in engineering in the world. In 2017, he became Doctor Honoris Causa at the University of Politehnica, Timisoara, Romania.